Optimal power extraction of a two-stage tidal turbine system based on backstepping disturbance rejection control

Xiuxing Yin[a], Xiaowei Zhao[b,] *

[a] School of Mechanical and Electrical Engineering, Guilin University of Electronic Technology, 541004 Guilin, P.R. China

[b] School of Engineering, University of Warwick, Coventry CV4 7AL, U.K.

*Corresponding author: xiaowei.zhao@warwick.ac.uk

Abstract

This paper investigates the optimal power generation control for a two-stage horizontal-axis tidal turbine system based on backstepping disturbance rejection control (BDRC), which is a new control framework for high-order nonlinear systems. The tidal turbine system is designed with the main structure being described. The dynamics of the tidal turbine system is then formulated based on the integration of the dynamics of its constitute components. The tidal turbine experiences large uncertainties and unknown dynamics from non-uniform operating thrust and fatigue forces, variations and turbulence in tidal flow velocities induced by waves and wind. The proposed BDRC is a unique control concept which has superior performance in dealing with these large uncertainties without requiring much information about the turbine dynamics. Consequently, the BDRC system is synthesized in two control loops for the control of the turbine dynamics (outer loop) and the q-axis current dynamics (inner loop) respectively to track the optimal tidal turbine speed and hence maintain the optimal power generations. Both the stability and convergence of the two closed control loops are subsequently analyzed and proved. The simulations are conducted in MATLAB/Simulink to compare the

performance of the developed BDRC system with a sliding mode control method used in the literature. In addition, the proposed BDRC algorithm is extended to a general nonlinear strict-feedback system with high uncertainties and external/internal disturbances. The proposed BDRC has significantly extended the traditional ADRC and does not need any differential operations, thereby totally eliminating the inherent problems of "explosion of complexity" and repeated differentiations of virtual control variables in traditional backstepping control.

Keywords:

Tidal turbine; Dynamic characteristics; Optimal power generation; Backstepping disturbance rejection control.

I. INTRODUCTION

Tidal turbines extract and convert kinetic energy from tidal streams (in open waters or channel-type areas) into electrical power in a similar way as wind turbines [1]. However, as the density of seawater is 1025 kg/m^3, about 837 times denser than air under standard atmospheric conditions, tidal turbines experience larger operating thrust and fatigue forces than wind turbines with the same dimension. Also, there are significant variations and turbulence in tidal flow velocities induced by waves and wind, and therefore the tidal loads across the rotor disc are not uniform and have large fluctuations. In addition, the submerged tidal turbine structures experience incredible levels of blade surface contamination and marine growth build-up for long periods of time [2]. All these differences pose serious challenges in controlling the rotor speed in a tidal turbine than in a wind turbine [3]. Moreover, the efficiency and power quality of the tidal turbines are still very low, which also require more effective control systems. Although advanced control methods have been widely used in wind turbine control [4], not much control effort has been conducted in the tidal energy field. Therefore, there is an need to introduce more advanced control algorithms to tidal turbine systems to improve their performances e.g., achieving higher efficiency and power quality, better regulation performances and greater robustness against the uncertainties and disturbances due to the turbines themselves and the tidal streams including swell effects and high turbulence.

In the literature, there are some research works on the control of tidal turbines. The sliding mode control design was proposed in [5, 6] for the optimal power generations and power regulations of a tidal turbine system with variable speed doubly-fed induction generator. Experimental verifications were conducted in a 7.5 kW real-time simulator that accounts for the resource and turbine models. However, this control system suffered from chattering effects caused by high-frequency control switching [6]. In [7], the optimal power control of a tidal turbine system (with a variable speed doubly fed induction generator) was designed with and without tidal current speed sensor. This control strategy relied highly on the resource and the tidal turbine models, whose sensitivity regarding swell effects needs to be analyzed. In [8], a maximum power point tracking control strategy for a tidal turbine system was presented for only low marine current speed, which was verified by simulation on a 10-kW generating system with a low-speed doubly salient permanent magnet generator of 50 rpm in MATLAB Simulink. In [9], the power control of a 1.5 MW tidal turbine was designed by considering the tuning chain as a part of the system's energetic macroscopic representation. The control of the machine side converter utilized optimal torque control for the maximum power point tracking and the minimization of generator power loss under the rated marine current speed. In [10], a fuzzy logic tuning based direct power control approach was proposed to achieve the optimal tidal power generation by using cascaded control loops. In [11], two model free reinforcement learning (RL) algorithms – Q-learning and Neural Fitted Q-iteration were proposed for the maximum power point tracking (MPPT) control of a tidal turbine. In [12], the ADV preview based nonlinear predictive control approach was proposed for a tidal turbine with continuously variable speed hydrostatic transmission to enhance the maximum tidal power generation. In [13], a sensor-less double integral sliding mode controller was designed for a hydrostatic tidal turbine to achieve the maximum power extraction in the presence of large parametric uncertainties and nonlinearities.

In general, to some extent, the aforementioned control methods may suffer from the disadvantages of relatively low reliability and low robustness particularly in the presence of large uncertain tidal current inputs. Other control techniques of tidal turbine systems [14] more or less relied on simple descriptions of a specific tidal system and were not extendable or difficult to apply in realistic and complex test field.

This paper considers the optimal power generation control of a two-stage horizontal-axis tidal turbine system. The optimal power control is based on backstepping disturbance rejection control (BDRC) algorithm which is an improved approach to traditional active disturbance rejection control (ADRC) [15]. The ADRC is a unique control concept and has superior performance in dealing with large uncertainties. The ADRC does not require much information about the plant dynamics, which is very easy to tune and thus very suitable for engineering implementation [16]. The energy savings and transient response features of the ADRC are also useful for the tidal energy generation. The ADRC has preliminarily been applied in a wide range of industrial applications, such as the hydraulic servo systems [17], the H-bridge DC-DC power converter [18], the permanent magnet synchronous motor [19], the flywheel energy storage system [20], the quadrotor trajectory tracking [21], the swift industrial implementations [22] and the open-cathode proton exchange membrane fuel cell [23].

Therefore, by utilizing the good disturbance rejection capability of the ADRC, this paper designs the BDRC by combining the feedforward arrangement and the ADRC to exploit the unique disturbance estimation and rejection capability of the ADRC in tidal turbine control. In the paper, the main characteristics of this tidal turbine system are analyzed by integrating all the dynamic equations of the constitute components. For tracking the optimal tidal turbine speed to maintain the optimum hydrodynamic efficiency, the BDRC is synthesized in two control loops including an outer turbine dynamics control loop and an inner q-axis current dynamics control loop. An extended state observer (ESO) and a nonlinear feedback controller are designed in each control loop. Both the stability and convergence of the two closed control loops and ESO are then analyzed accordingly. The proposed BDRC is also extended to general nonlinear strict-feedback system with high uncertainties and external/internal disturbances. Simulations are conducted based on the developed 160 kW tidal turbine system in MATLAB/Simulink to assess the performance of the developed BDRC algorithm by comparing it with the sliding mode control method.

The proposed BDRC does not need accurate model information and features inherent robustness and high accuracy against various disturbances and internal/external uncertainties. Each step BDRC of the nonlinear strict feedback system is highly self-independent, self-convergent and self-stabilized, which together form the stability of the closed loop system. The proposed BDRC design does not need any differentials and hence does not suffer from the risks of explosion of complexity and high computational burden either. Actually, each step BDRC has fixed control structure and is easy to implement since only some control coefficients are needed to be re-tuned between different steps for general strict feedback systems.

The main novelty and contributions of the work are listed as follows:

1) Designing the BDRC in two control loops including an outer turbine dynamics control loop and an inner

q-axis current dynamics control loop.

2) The proposed BDRC is also extended to general nonlinear strict-feedback system with high uncertainties and external/internal disturbances.

3) The performance of the developed BDRC algorithm is verified based on a 160 kW tidal turbine system by comparing it with the sliding mode control method.

Following the introduction section, the section II describes the two-stage tidal turbine system. The section III presents the dynamic characteristics and optimal power generation of the tidal turbine. The section IV details the BDRC design. The section V presents the verifications and discussions of the proposed BDRC in tidal turbine control, and the section VI provides the conclusions of the work.

II. THE TWO-STAGE TIDAL TURBINE SYSTEM

The horizontal-axis type tidal turbine system is considered as one of the most promising options for improving tidal power extraction and efficiency [24]. A model 160 kW two-stage tidal turbine system is developed in this section. As illustrated in Fig. 1, the designed tidal turbine system mainly consists of a variable-speed tidal stream turbine, a compact drive train, a permanent magnet synchronous generator (PMSG), a power converter and electric load. The drive train consists of a low-speed shaft, a small-sized gear train and a high-speed shaft that connected to the PMSG. Its first stage refers to the tidal turbine, low-speed shaft and gear train, whereas the second stage consists of the high-speed shaft and PMSG.

Tidal turbine blades are driven by incoming tidal streams which have slowly time-varying velocities by nature. The captured mechanical energy from the tidal turbine is transferred to the PMSG for electrical power generation via the small-sized gear train. The stator windings of the PMSG are connected to the power converter which is then cascaded by an electric load or grid side power converter. The generator-side power converter is actually a control actuator for power transformations between AC and DC, and therefore is a main element for implementing control actions for power maximizations of the tidal turbine system.

The electricity generation from the PMSG typically requires relatively steady and fast drive-train rotations whereas the tidal stream and turbine speeds are usually slow and intermittent. Thus, the small-sized gear train and PMSG are employed here to significantly accelerate the turbine rotations and efficiently generate electrical energy at relatively low cost. The gear train also has a relatively small transmission ratio and the PMSG has high power density, which makes the system highly compact and efficient.

This two-stage configuration not only significantly reduces the size and weight of a conventional PMSG tidal turbine system which is configured with a low-speed direct drive, but also can considerably increase the efficiency of the PMSG since this will always enable the PMSG work in its relatively high-speed ranges and high-efficiency characteristic areas.

In practice, all the components of this two-stage tidal turbine system except for the turbine blades and power converter will be encased in a seawater proof housing and then deeply submerged underwater for capturing high-speed tidal streams. The power converter and the associated control elements will be naturally located onshore for power regulations and central control.

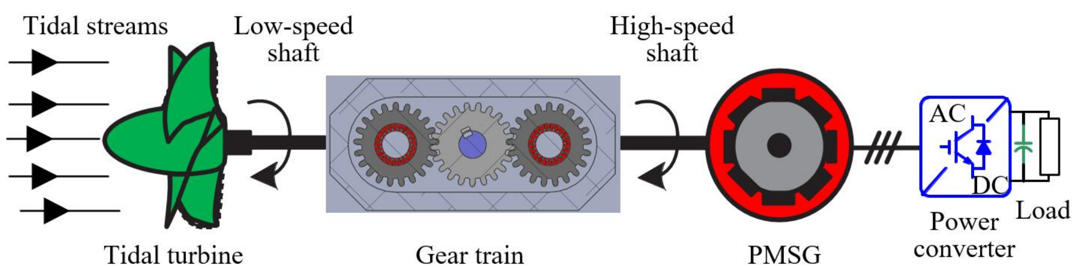

Fig. 1 Schematic of the two-stage tidal turbine system

III. DYNAMIC CHARACTERISTICS AND OPTIMAL POWER GENERATION

The dynamic characteristics of the 160-kW tidal turbine system described in Section II is modeled in this section, by integrating all the dynamic equations of its constitute components.

A. Tidal Streams

Even though the tidal stream velocity is highly predictable and relatively slowly time-varying, short-term tidal stream velocity is still stochastic and fluctuating due to interactions among tidal currents, water depth, ocean terrain, waves and winds. One of the most influencing factor is the wave field and hence the realistic tidal stream speed v can be well simulated by the sum of a uniform term v_t and a wave induced non-uniform term v_w [25]. Thus,

$$v_t = \begin{cases} 1.1\left(1+\dfrac{z}{h}\right)^{1/7} v_{t\max} \text{ for } -1 \le \dfrac{z}{h} \le -0.5 \\ v_{t\max} \text{ for } \dfrac{z}{h} \ge -0.5 \end{cases} \quad (1)$$

where z is the depth of the tidal system from seawater surface, h is the total the water depth (m), $v_{t\max}$ is the maximum tidal stream velocity (m/s).

The non-uniform term v_w due to the existence of a surface wave is given by

$$v_w(y,t) = \frac{\xi\varpi \cosh\left[k(z+h)\right]}{\sinh(kh)}\cos(\varpi t) \quad (2)$$

where t is the elapsed time, ξ is the wave height (m), ϖ is the wave frequency (rad/s), and k is the wave number.

The wave frequency ϖ in (2) can be reasonably designed to represent swell effects or tidal speed oscillations in actual tidal streams. To this end, several frequency components should be added together to simulate a realistic swell effect based on a specified swell spectrum.

In practice, the inflow profile of actual tidal stream speed can be measured upstream of the tidal turbine rotor by using Acoustic Doppler Velocimetry (ADV) due to its great operational flexibility and lower cost [26].

B. Tidal Turbine Dynamics

The tidal stream speeds are used for calculating the hydrodynamic torque T_t and power of a tidal turbine P_t.

$$\begin{cases} T_t = \dfrac{1}{2}\rho\pi R^3 v^2 \dfrac{C_p}{\lambda} \\ P_t = \dfrac{1}{2}\rho\pi R^2 v^3 C_p \end{cases} \quad (3)$$

where ρ is the seawater density (1025 kg/m^3), R is the turbine blade radius (m), λ is an unit-less tip speed ratio which is a characteristic factor for the tidal turbine. C_p is the tidal power conversion coefficient. It is the ratio of the mechanical power of the tidal turbine to the power conveyed by the tidal streams through the swept area of the turbine rotor and thus expresses the ability of the tidal turbine to extract kinetic energy from the moving seawater. For a fixed pitch tidal turbine (like the one considered in this paper), C_p can be derived based on fitting function of the tip speed ratio as follows

$$\begin{cases} C_p = 0.555\left(\dfrac{116}{\kappa} - 5\right) e^{\left(\frac{-20}{\kappa}\right)} \\ \kappa = \dfrac{1}{1/\lambda - 0.035} \end{cases} \tag{4}$$

where κ is an intermediate constant.

The tip speed ratio λ is typically expressed as the ratio of the blade tip speed to the free stream speed

$$\lambda = \frac{\omega_t R}{v} \tag{5}$$

where ω_t denotes the rotating speed of the tidal turbine.

C. Two-stage Drive Train

The dynamics of this two-stage drive train are described by a two-mass model (see Fig. 2):

$$\begin{cases} J_t \dot{\omega}_t = T_t - k_t \omega_t - T_L \\ J_g \dot{\omega}_g = T_h - T_g - k_g \omega_g \end{cases} \tag{6}$$

where J_t and J_g are the inertias of the tidal turbine and generator, respectively, T_L and T_h are the torques at the gearbox ends of the low-speed and high-speed shafts, respectively, T_g and ω_g are the electromagnetic torque and rotating speed of the PMSG, respectively, and k_t and k_g are the friction damping coefficients of the low-speed and high-speed shafts, respectively.

The torque at the gearbox end of the low-speed shaft is represented as

$$T_L = k_{ls}\left(\theta_t - \theta_{ls}\right) + b_{ls}\left(\omega_t - \omega_{ls}\right) \tag{7}$$

where k_{ls} and b_{ls} the low-speed shaft stiffness and damping coefficient, respectively, θ_t and ω_t are respectively the rotor side angular deviation and shaft speed, θ_{ls} and ω_{ls} are respectively the gearbox side angular deviation and shaft speed.

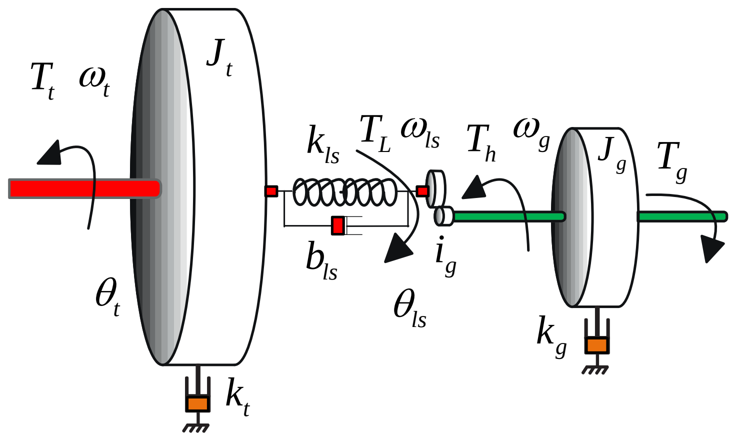

Fig. 2 Two mass model of the two-stage drive train

The variables between the low-speed and high-speed sides are related as

$$\begin{cases} T_L \omega_{ls} = T_h \omega_g \\ i_g = \dfrac{T_L}{T_h} \end{cases} \tag{8}$$

where i_g is the transmission ratio of the gear train.

For the scale of the tidal turbine considered here (i.e., 160 kW), the low-speed shaft can be assumed to be a rigid body. i.e., $\omega_t = \omega_{ls}$. Then its drive train model can be derived by combining the above equations (6)-(8):

$$\left(J_t + J_g i_g^2\right)\dot{\omega}_t = T_t - T_g i_g - \left(k_t + k_g i_g^2\right)\omega_t \tag{9}$$

D. PMSG Dynamics

The PMSG dynamic equations are always expressed in the d–q coordinate frame rotating synchronously with the magnet flux. The electromagnetic torque T_g in the PMSG can be formulated as

$$T_g = \frac{3}{2} p\psi i_{sq} \tag{10}$$

where p is the number of pole pairs, ψ is the magnet flux, i_{sq} is the stator q-axis current component.

As shown in (10), the stator q-axis current component is used to develop generator torque since both p and ψ are constant at steady state. Hence, the control of the tidal turbine speed ω_t can be reasonably achieved by implementing adequate actions for i_{sq} as indicated in (9) and (10).

The Park model of the electrical dynamics of the PMSG in terms of q-axis voltage and current is

$$\frac{\mathrm{d}i_{sq}}{\mathrm{d}t} = -\frac{R_s}{L_s} i_{sq} - \frac{p i_g \psi}{L_s} \omega_t - p\omega_g i_{sd} + \frac{u_{sq}}{L_s} \tag{11}$$

where R_s and L_s are the resistance and inductance of the stator winding, respectively, u_{sq} is the q-component of instant stator voltage, i_{sd} is the d-component of instant stator current.

The equation (11) shows that the q-axis stator current can be tuned to its desired values by regulating the q-component of the instant stator voltage. Meanwhile, the direct-axis current component can be tuned to zero to minimize demagnetization for a given torque, and therefore, reduce stator flux and minimize resistive and core losses [27]. Since this paper focuses on the optimal generator power through torque control, only the q-axis control variables will be considered.

E. Optimal Power Generation

The optimal power generation control of the 160-kW tidal turbine system aims to extract the maximum available tidal power by keeping the turbine power coefficient at the maximum values below the rated tidal flow speed of 2 m/s. To this end, the tidal turbine should be operated in variable-speed mode to track the optimal tidal turbine speed corresponding to the maximum power coefficient so that the optimum hydrodynamic efficiency is maintained.

The optimal tidal turbine speed ω_{optf} can be designed as

$$\omega_{optf} = \frac{1}{\tau s+1}\frac{\lambda_{opt} v}{R} \tag{12}$$

where $\lambda_{opt} = 8$ denotes the optimal tip speed ratio in accordance with the maximum power coefficient, s is the Laplace operator, τ =0.02 s denotes the filter constant and the filter in (12) is used to eliminate any swell effect, the tidal stream speed v can be acquired by using ADV measurements in advance.

At the optimal power generation point, the optimal generator power P_{opt} is

$$P_{opt} = k_{opt}\omega_{optf}^3 \tag{13}$$

where

$$k_{opt} = \frac{1}{2}\frac{\pi R^5 \rho}{\lambda_{opt}^3} C_p\left(\lambda_{opt}\right) \tag{14}$$

IV. THE BDRC DESIGN

The BDRC system of the developed 160 kW tidal turbine system works in a backstepping manner and involves two cascaded control loops: the first control loop for the turbine dynamics (9), and the second control loop for the q-axis PMSG dynamics (11). The former aims to track the optimal tidal turbine speed by generating reference electromagnetic torque or equivalently the reference q-axis current as indicated in (10), while the latter ensures that the reference q-axis current is reached in finite time. Each control loop will be designed based on an extended state observer (ESO) and a nonlinear feedback controller. The stability and convergence of both (closed) control loops and ESO will be analyzed accordingly.

A. BDRC Design of the Tidal Turbine

The tidal turbine dynamics in (9) can be re-formulated as

$$\dot{\omega}_t = \frac{T_t - \left(k_t + k_g i_g^2\right)\omega_t}{J_t + J_g i_g^2} - \frac{3p\psi i_g}{2\left(J_t + J_g i_g^2\right)} i_{sq} \tag{15}$$

The above dynamics (15) can be re-structured into a two-degree-of freedom configuration. Thus,

$$\begin{cases} \dot{x}_{11} = x_{21} + b_{01} i_{sq}; \\ \dot{x}_{21} = \dot{f}_1(v, \omega_t). \end{cases} \tag{16}$$

where

$$\begin{cases} x_{11} = \omega_t; \\ x_{21} = f_1(v, \omega_t) = \dfrac{T_t - \left(k_t + k_g i_g^2\right)\omega_t}{J_t + J_g i_g^2} + \Delta_1. \end{cases} \tag{17}$$

$f_1(v, \omega_t)$ denotes the combination of the unknown dynamics and disturbances, which arise from the non-uniform operating thrust and fatigue forces, variations and turbulence in tidal flow velocities induced by waves and wind, and additional loads from blade surface contamination and marine growth build-up. Δ_1 denotes modelling differences between the tidal turbine model and the actual tidal turbine dynamics, b_{01} is the normal value of $-\dfrac{3p\psi i_g}{2\left(J_t + J_g i_g^2\right)}$.

1) ESO Design

The ESO is essential for observing unknown states and disturbances in real time for the BDRC design.

Define the state estimation errors as

$$\begin{cases} \varepsilon_{11} = \hat{x}_{11} - x_{11}; \\ \varepsilon_{21} = \hat{x}_{21} - x_{21}. \end{cases} \tag{18}$$

where ε_{11} and ε_{21} denote the state estimation errors by the observer, and $\hat{x}_{11}$ and $\hat{x}_{21}$ denote the state estimates.

Design the ESO as

$$\begin{cases} \dot{\hat{x}}_{11} = \hat{x}_{21} + b_{01} i_{sq} - \beta_{11} fal\left(\varepsilon_{11}, \vartheta_{11}, \eta_{11}\right); \\ \dot{\hat{x}}_{21} = -\beta_{21} fal\left(\varepsilon_{11}, \theta_{11}, \eta_{11}\right). \end{cases} \tag{19}$$

where β_{11} and β_{21} are the observer gains, $fal(\cdot)$ is a nonlinear core function used in the BDRC, for example, the function $fal\left(\varepsilon_{11}, \vartheta_{11}, \eta_{11}\right)$ can be defined as

$$fal\left(\varepsilon_{11},\vartheta_{11},\eta_{11}\right)=\begin{cases}\varepsilon_{11}/\eta_{11}^{1-\vartheta_{11}}, & \left|\varepsilon_{11}\right|\le\eta_{11}\\ \left|\varepsilon_{11}\right|^{\vartheta_{11}}\operatorname{sigm}\left(\varepsilon_{11}\right), & \left|\varepsilon_{11}\right|>\eta_{11}\end{cases} \tag{20}$$

where ϑ_{11},η_{11} are two tunable control coefficients with $0<\vartheta_{11}<1$. The function $\operatorname{sigm}\left(\varepsilon_{11}\right)$ is defined as

$$\operatorname{sigm}\left(\varepsilon_{11}\right)=\frac{1-\exp\left(-\mu\varepsilon_{11}\right)}{1+\exp\left(-\mu\varepsilon_{11}\right)} \tag{21}$$

where μ is a positive gain, when $\mu\to\infty$, the sigm(•) function will eventually converge to the well-known sign(•) function in finite time.

The observer error dynamics by subtracting (16) from (19) are

$$\begin{cases}\dot{\varepsilon}_{11}=\varepsilon_{21}-\beta_{11}fal\left(\varepsilon_{11},\vartheta_{11},\eta_{11}\right);\\ \dot{\varepsilon}_{21}=-\dot{f}_{1}\left(v,\omega_{t}\right)-\beta_{21}fal\left(\varepsilon_{11},\theta_{11},\eta_{11}\right).\end{cases} \tag{22}$$

***Proof of convergence**:* In order to verify the convergence of the ESO, define two boundary functions $g_{11}\left(\varepsilon_{11}\right)$ and $g_{21}\left(\varepsilon_{11},\varepsilon_{21}\right)$ as follows:

$$\begin{cases}g_{11}\left(\varepsilon_{11}\right)\ge\dot{\varepsilon}_{11}+\beta_{11}g_{11}\left(\varepsilon_{11}\right)\operatorname{sigm}\left(\varepsilon_{11}\right);\\ g_{21}\left(\varepsilon_{11},\varepsilon_{21}\right)=\dot{\varepsilon}_{21}+\beta_{21}g_{21}\left(\cdot\right)\operatorname{sigm}\left(\varepsilon_{21}\right).\end{cases} \tag{23}$$

Define a Lyapunov function

$$V_{11}\left(\varepsilon_{11},\varepsilon_{21}\right)=\frac{1}{2}\varepsilon_{11}^{2}+\frac{1}{2}\varepsilon_{21}^{2} \tag{24}$$

By combining (22), (23) and (24), the time derivative of (24) is given by

$$\begin{aligned}&\dot{V}_{11}\left(\varepsilon_{11},\varepsilon_{21}\right)=\varepsilon_{11}\dot{\varepsilon}_{11}+\varepsilon_{21}\dot{\varepsilon}_{21}\\ &\le\varepsilon_{11}\left[g_{11}\left(\varepsilon_{11}\right)-\beta_{11}g_{11}\left(\varepsilon_{11}\right)\operatorname{sigm}\left(\varepsilon_{11}\right)\right]\\ &+\varepsilon_{21}\left[g_{21}\left(\varepsilon_{11},\varepsilon_{21}\right)-\beta_{21}g_{21}\left(\cdot\right)\operatorname{sigm}\left(\varepsilon_{21}\right)\right]\\ &\le\varepsilon_{11}g_{11}\left(\varepsilon_{11}\right)\left[1-\beta_{11}\operatorname{sigm}\left(\varepsilon_{11}\right)\right]\\ &+\varepsilon_{21}g_{21}\left(\cdot\right)\left[1-\beta_{21}\operatorname{sigm}\left(\varepsilon_{21}\right)\right]\le\\ &\left(1-\beta_{11}\right)\left|\varepsilon_{11}\right|g_{11}\left(\varepsilon_{11}\right)+\left(1-\beta_{21}\right)\left|\varepsilon_{21}\right|g_{21}\left(\cdot\right)\end{aligned} \tag{25}$$

By selecting $\beta_{11}>1$ and $\beta_{21}>1$, the function $\dot{V}_{11}\left(\varepsilon_{11},\varepsilon_{21}\right)$ is negative semidefinite. Since $V_{11}\left(\varepsilon_{11},\varepsilon_{21}\right)$ is positive definite, there exists $0 \le V_{11}(\varepsilon_{11}, \varepsilon_{21}) \le V_{11}(0,0)$. Thus, $V_{11}(\varepsilon_{11}, \varepsilon_{21})$ is bounded. Hence, all the state estimates in (19) and the estimation errors in (18) are globally uniformly bounded. Based on Barbalat's lemma [28], it's easy to conclude that estimation errors in (18) converge to zero in finite time.

2) Nonlinear Feedback Controller Design

To accurately track the optimal tidal turbine speed ω_{optf}, the nonlinear feedback controller is designed based on the ESO with control variable being the reference q-axis stator current i_{sq_ref}.

Define the speed tracking errors as

$$\begin{cases} e_1 = \omega_{optf} - \hat{x}_{11} = s_1 - \varepsilon_{11}; \\ s_1 = \omega_{optf} - x_{11}. \end{cases} \tag{26}$$

Based on the tracking errors in (26), the controller is

$$i_{sq\_ref} = \alpha_1 fal(e_1, \sigma_1, \delta_1) - \hat{x}_{21}/b_{01} \tag{27}$$

where α_1, σ_1 and δ_1 are tunable control coefficients used to shape the nonlinear core function and achieve the desired control actions.

Define the tracking error for the reference q-axis current in (27) as

$$s_2 = i_{sq\_ref} - i_{sq} \tag{28}$$

Substituting (27) and (28) into (16) yields

$$\dot{x}_{11} = b_{01}\alpha_1 fal(e_1, \sigma_1, \delta_1) - b_{01}s_2 - \varepsilon_{21} \tag{29}$$

Hence, the time derivative of s_1 is formulated as

$$\begin{aligned} \dot{s}_1 &= \dot{\omega}_{optf} - \dot{x}_{11} \\ &= \dot{\omega}_{optf} - b_{01}\alpha_1 fal(e_1, \sigma_1, \delta_1) + b_{01}s_2 + \varepsilon_{21} \end{aligned} \tag{30}$$

Proof of stability: To prove the stability of the controller in (27), the following Lyapunov function $V_{21}(e_1)$ is defined as

$$V_{21}(e_1) = \frac{1}{2}e_1^2 = \frac{1}{2}(s_1 - \varepsilon_{11})^2 \tag{31}$$

By considering (22), the time derivative of (31) is

$$\begin{aligned}
\dot{V}_{21}(e_1) &= (s_1-\varepsilon_{11})(\dot{s}_1-\dot{\varepsilon}_{11}) \\
&= (s_1-\varepsilon_{11})\begin{bmatrix}\dot{\omega}_{optf}-b_{01}\alpha_1 fal(e_1,\sigma_1,\delta_1)+b_{01}s_2+\varepsilon_{21} \\ -(\varepsilon_{21}-\beta_{11} fal(\varepsilon_{11},\vartheta_{11},\eta_{11}))\end{bmatrix} \\
&= (s_1-\varepsilon_{11})\begin{bmatrix}\dot{\omega}_{optf}-b_{01}\alpha_1 fal(e_1,\sigma_1,\delta_1) \\ +b_{01}s_2+\beta_{11} fal(\varepsilon_{11},\vartheta_{11},\eta_{11})\end{bmatrix} \\
&= -b_{01}\alpha_1(s_1-\varepsilon_{11})\, fal((s_1-\varepsilon_{11}),\sigma_1,\delta_1) \\
&\quad +(s_1-\varepsilon_{11})\left[\dot{\omega}_{optf}+b_{01}s_2+\beta_{11} fal(\varepsilon_{11},\vartheta_{11},\eta_{11})\right]
\end{aligned} \tag{32}$$

Since $fal(e_1,\sigma_1,\delta_1)$ is an odd and monotonically increasing function, the first term $(s_1-\varepsilon_{11})\, fal((s_1-\varepsilon_{11}),\sigma_1,\delta_1)\geq 0$ in (32). In practice, the other terms e_1, $\dot{\omega}_{optf}$ and s_2 are ultimately bounded when considering the actual control system.

Hence, (32) is re-written as

$$\dot{V}_{21}(e_1)\leq -b_{01}\alpha_1(s_1-\varepsilon_{11})\, fal((s_1-\varepsilon_{11}),\sigma_1,\delta_1)+B \tag{33}$$

where B is a boundary and can be defined as

$$B\geq (s_1-\varepsilon_{11})\left[\dot{\omega}_{optf}+b_{01}s_2+\beta_{11} fal(\varepsilon_{11},\vartheta_{11},\eta_{11})\right]. \tag{34}$$

As indicated in (33), by appropriately selecting relatively large value for the control parameter α_1, there exists $\dot{V}_{21}(e_1)\leq 0$, and hence the nonlinear closed control loop is stable and all the tracking errors converge to zero eventually.

B. BDRC Design of the Current Control Loop

The BDRC design of the q-axis current control loop follows the same procedures as that for the tidal turbine dynamics.

The two-degree-of freedom state space representation of the q-axis current dynamics (11) is defined as

$$\begin{cases}\dot{x}_{12} = x_{22}+b_{02}u_{sq}; \\ \dot{x}_{22} = \dot{f}_2(i_{sq},i_{sd},\omega_t).\end{cases} \tag{35}$$

where

$$\begin{cases} x_{12} = i_{sq}; \\ x_{22} = f_2\left(i_{sq}, i_{sd}, \omega_t\right) = -\dfrac{R_s}{L_s} i_{sq} - \dfrac{p i_g \psi}{L_s} \omega_t - p\omega_g i_{sd} + \Delta_2. \end{cases} \tag{36}$$

$f_2\left(i_{sq}, i_{sd}, \omega_t\right)$ denotes the lumped uncertainties of the unknown current dynamics and disturbances including d-axis current loop dynamics, Δ_2 denotes the lumped modelling errors in the current control loop, b_{02} is the known and normal value of $\dfrac{1}{L_s}$.

The ESO for the q-axis current loop is designed as follows.

Define the state estimation errors as

$$\begin{cases} \varepsilon_{12} = \hat{x}_{12} - x_{12}; \\ \varepsilon_{22} = \hat{x}_{22} - x_{22}. \end{cases} \tag{37}$$

where ε_{12} and ε_{22} denote the state estimation errors by the observer, $\hat{x}_{12}$ and $\hat{x}_{22}$ denote the state estimates.

Design the ESO as

$$\begin{cases} \dot{\hat{x}}_{12} = \hat{x}_{22} + b_{02} u i_{sq} - \beta_{12} fal\left(\varepsilon_{12}, \vartheta_{12}, \eta_{12}\right); \\ \dot{\hat{x}}_{22} = -\beta_{22} fal\left(\varepsilon_{12}, \theta_{12}, \eta_{12}\right). \end{cases} \tag{38}$$

where β_{12} and β_{22} are observer gains, $fal\left(\varepsilon_{12}, \theta_{12}, \eta_{12}\right)$ is a nonlinear core function used in the BDRC, $\vartheta_{12}, \theta_{12}, \eta_{12}$ are tunable control coefficients with $0 < \vartheta_{12} < 1$.

The nonlinear feedback controller can also be synthesized as follows.

Define the q-axis current tracking errors as

$$e_2 = i_{sq\_ref} - \hat{x}_{12} = s_2 - \varepsilon_{12} \tag{39}$$

Based on the tracking errors in (28) and (39), the nonlinear current controller is designed as

$$u_{sq} = \alpha_2 fal\left(e_2, \sigma_2, \delta_2\right) - \hat{x}_{22} / b_{02} \tag{40}$$

where α_2, σ_2 and δ_2 are tunable control coefficients used to achieve the desired reference q-axis current.

C. Extended BDRC Control Framework

The proposed BDRC system can also be well extended to general nonlinear strict-feedback system with high uncertainties and external/internal disturbances. The *n*-th order strict-feedback nonlinear system can be represented in the following form:

$$\begin{cases} \dot{x}_1 = f_1\left(x_1\right) + g_1\left(x_1\right) x_2 \\ \dot{x}_2 = f_2\left(x_1, x_2\right) + g_2\left(x_1, x_2\right) x_3 \\ \cdots \\ \dot{x}_i = f_i\left(x_1, x_2, .., x_{i-1}\right) + g_i\left(x_1, x_2, .., x_{i-1}\right) x_{i+1} \\ \cdots \\ \dot{x}_n = f_n\left(x_1, x_2, .., x_{n-1}\right) + g_n\left(x_1, x_2, .., x_{n-1}\right) u \\ y = x_1. \end{cases} \tag{41}$$

where x, y and u denote system state, output and control input, respectively, $f_i\left(x_1, x_2, .., x_{i-1}\right)$ denotes unknown smooth function representing lumped system uncertainties and disturbances, $g_i\left(x_1, x_2, .., x_{i-1}\right)$ denotes smooth control-gain function.

For the BDRC design, the typical *i*-th subsystem in this nonlinear system can be rearranged into a two-degree of freedom system as follows

$$\begin{cases} \dot{x}_{1i} = x_{2i} + b_{0i} x_{i+1}; \\ \dot{x}_{2i} = f_{ai}\left(x_1, x_2, .., x_{i-1}\right). \end{cases} \tag{42}$$

where

$$\begin{cases} x_{1i} = x_i; \\ x_{2i} = f_{ai}\left(\cdot\right) = f_i\left(x_1, x_2, .., x_{i-1}\right) + \Delta_i. \end{cases} \tag{43}$$

$f_{ai}\left(\cdot\right)$ denotes the lumped combination of unknown uncertainties, disturbances and un-modelled dynamics, Δ_i denotes modelling errors, b_{01} is the nominal, steady state or boundary value of the gain function $g_i\left(x_1, x_2, .., x_{i-1}\right)$.

For designing an ESO for the system (42), define the following state estimation errors

$$\begin{cases} \varepsilon_{1i} = \hat{x}_{1i} - x_{1i}; \\ \varepsilon_{2i} = \hat{x}_{2i} - x_{2i}. \end{cases} \tag{44}$$

where ε_{1i} and ε_{2i} denote the state estimation errors by the observer, $\hat{x}_{1i}$ and $\hat{x}_{2i}$ denote the state estimates.

Design the ESO as

$$\begin{cases} \dot{\hat{x}}_{1i} = \hat{x}_{2i} + b_{0i} x_{i+1} - \beta_{1i}\, fal\left(\varepsilon_{1i}, \vartheta_{1i}, \eta_{1i}\right); \\ \dot{\hat{x}}_{2i} = -\beta_{2i}\, fal\left(\varepsilon_{1i}, \theta_{1i}, \eta_{1i}\right). \end{cases} \tag{45}$$

where β_{1i} and β_{2i} are ESO gains, $\vartheta_{1i}, \theta_{1i}, \eta_{1i}$, σ_i and δ_i are tunable control coefficients with $0 < \vartheta_{1i} < 1$.

For the nonlinear feedback control design of the system (42), define the *i*-th subsystem tracking errors as

$$\begin{cases} e_i = x_{i\_ref} - \hat{x}_{1i} = s_i - \varepsilon_{1i}; \\ s_i = x_{i\_ref} - x_{1i}. \end{cases} \tag{46}$$

where x_{i_ref} denotes the reference value for the *i*-th subsystem, which can be derived from the (*i*-1)-th subsystem based on the BDRC.

Based on the tracking errors in (46), the nonlinear feedback controller is designed as

$$x_{i+1\_ref} = \alpha_i\, fal\left(e_i, \sigma_i, \delta_i\right) - \hat{x}_{2i} / b_{0i} \tag{47}$$

where α_i, σ_i and δ_i are tunable control coefficients for tracking the desired reference inputs, x_{i+1_ref} denotes the control input for the *i*-th subsystem or the reference input for the (*i*+1)-th subsystem.

The BDRC design for each subsystem is totally independent and the BDRC for other subsystems in (41) follow the same way as that in (42)-(47). Additionally, the proofs of stability and convergence of the nonlinear feedback controller and ESO also follow the similar ways as that in section IV-A.

The tuning of the BDRC control parameters should make the core function $fal(\cdot)$ hold the characteristics of “small error, big gain; big error, small gain” so that tracking or estimation errors can be mitigated in real time. The control gains α_i, β_{1i} and β_{2i} should be chosen relatively large to achieve fast response, whereas $\vartheta_{12}, \theta_{12}, \eta_{12}, \sigma_i$ and δ_i should be tuned relatively small to achieve the desired accuracy. The selection of the control parameters should also ensure that the function $\dot{V}_{11}\left(\varepsilon_{11},\varepsilon_{21}\right)\le 0$, $\dot{V}_{21}\left(e_1\right)\le 0$. In addition, many intelligent optimization approach can also be used to obtain the optimal control and observer parameters such as the chaotic grey wolf optimization (CGWO) algorithm [21].

The BDRC does not need any differential operations so that the tracking differentiator and simultaneous tracking of each state in traditional ADRC [29] are not required in BDRC. The BDRC differs significantly from the traditional backstepping control and does not have the inherent problems of "explosion of complexity" and repeated differentiations of virtual control variables [30]. The proposed BDRC approach is also different from the recently proposed backstepping technique based ADRC approach in which the derivative of the virtual control variable needs to be approximated and the activations of the ESOs are delayed successively [31].

V. VERIFICATIONS AND DISCUSSIONS

The simulations were conducted based on the developed 160 kW tidal turbine system in MATLAB/Simulink to comparatively evaluate the effectiveness of the BDRC with the sliding mode control method developed in [5]. The data for the tidal stream speed was obtained from the East China Sea and coincides well with the model in (1) and (2). The rated tidal current speed is 2 m/s and the rated tidal turbine speed is 3.5 rad/s. The main design parameters for the tidal turbine system and BDRC are: $J_t=1\times10^4 kg\cdot m^2$, $J_g=10kg\cdot m^2$, $i_g=30$, $k_t=k_g=0.3$, $R=5m$, $\alpha_1=-22167$, $\alpha_2=400$, σ_1,σ_2, δ_1 and δ_2 can be chosen between 1×10^{-2} and 1×10^{-8}, respectively. In order to ensure the fair comparison, the performances of the two controllers are tuned to their best and then they are compared under the same operating conditions.

As illustrated in Fig. 3, the tidal stream speed increases from 0.1 m/s to around 1.8 m/s and then remains relatively steady between 1.6 m/s and 2 m/s. The speed variations represent a realistic tidal stream profile and include surface wave effects.

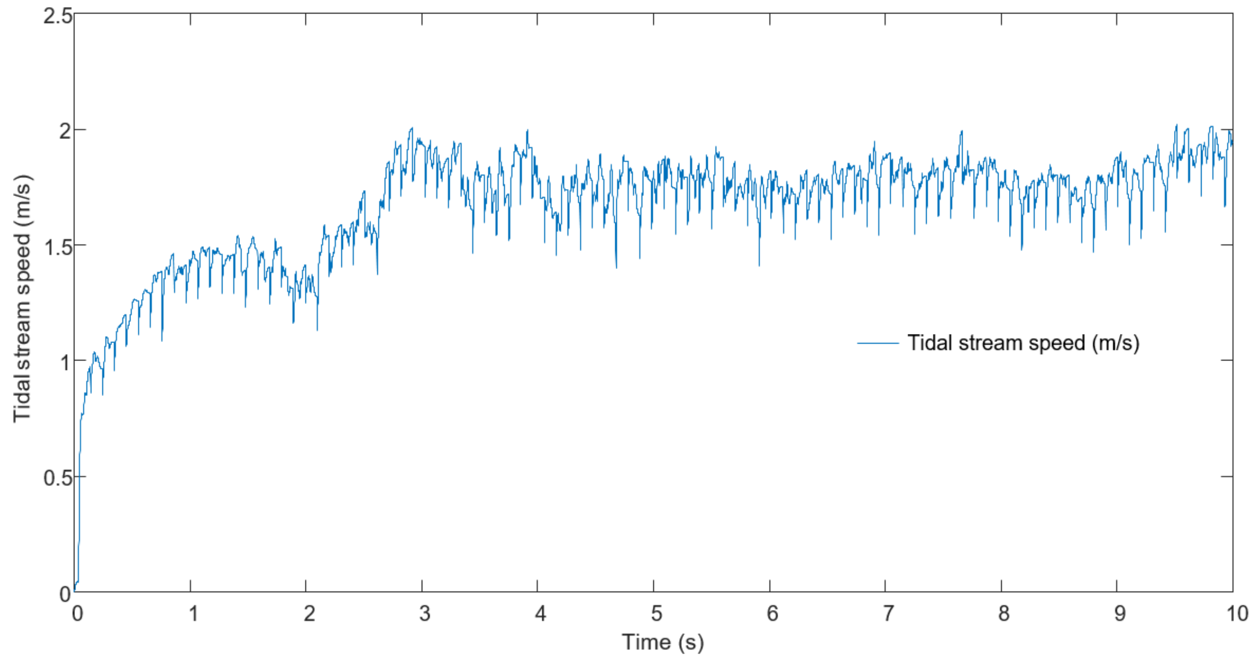

Fig. 3 Tidal stream speed variations

As shown in Fig. 4, the tidal turbine speed can be well regulated at the optimal speed by the BDRC, whereas it exhibits some variations and cannot track the optimal values well when using the sliding mode control. This indicates that the BDRC can be used to more accurately track the optimal tidal turbine speeds.

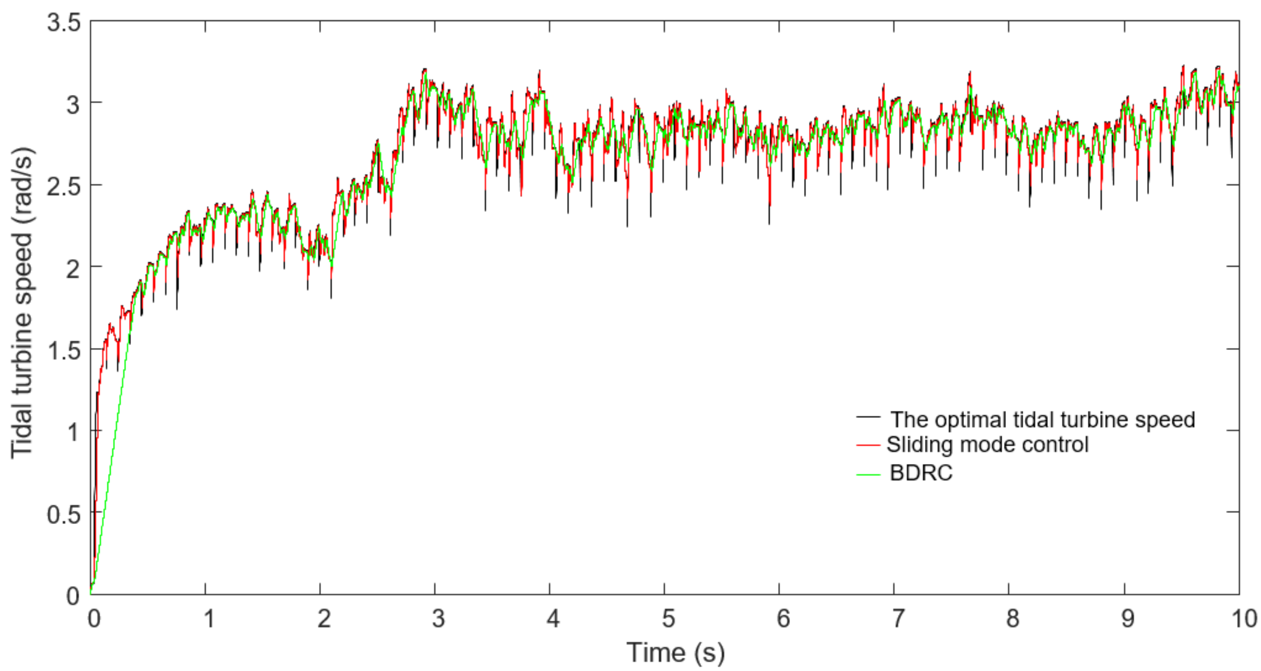

Fig. 4 Tidal turbine speed variations

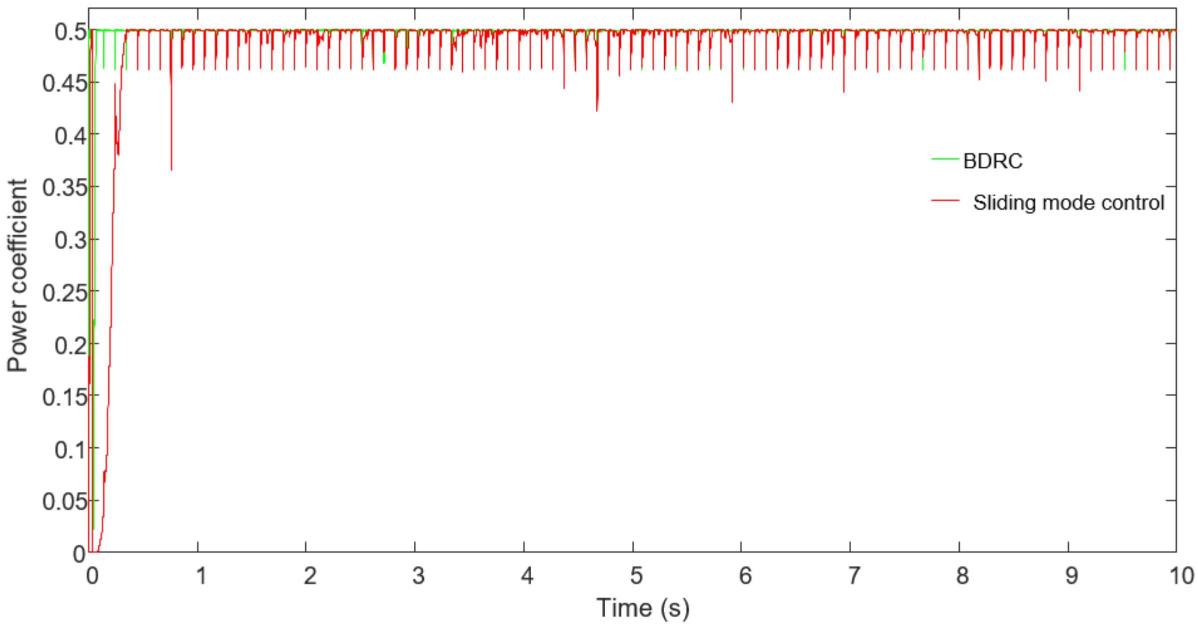

Fig. 5 Power coefficient comparisons

As illustrated in Fig. 5, the power coefficient can be well maintained around the maximum value of 0.5 by using BDRC, whereas the power coefficient sometimes deviates from the desired value when using the sliding mode control. Thus, the tidal power efficiency can be more effectively maintained by using the BDRC.

As described in Fig. 6, the power generation of the tidal turbine system tracks the optimal power profile more accurately by using BDRC than using sliding mode control. The large and high-frequency power fluctuations (due to control switch) in the case of sliding mode control may excite un-modeled high frequency modes, cause undesirable power consumptions and potential performance degradations of the system. In addition, the sliding mode control method employed needs very accurate turbine torque estimates, which is difficult to achieve in practice.

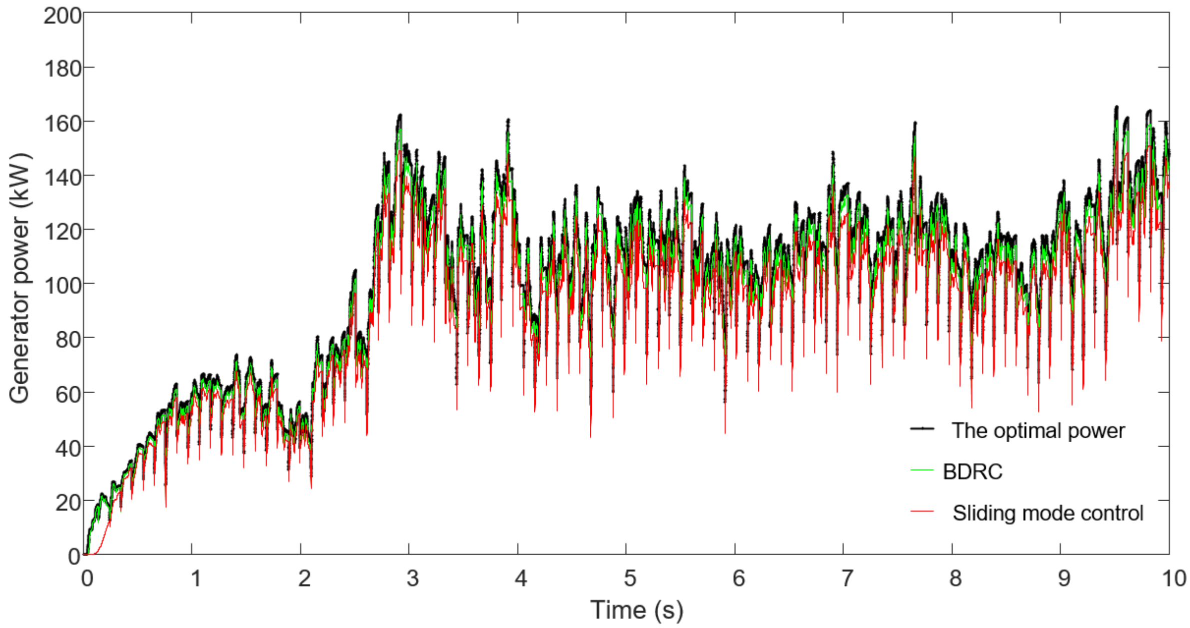

Fig. 6 Generator power variations

By observing the above results, it is clear that the proposed BDRC can be used to more accurately track the optimal tidal turbine speed and therefore maintain the relatively higher tidal power efficiency than the sliding mode control method. The variations of the tidal turbine speed and generator power when using the BDRC are smoother than the case when the sliding mode control method is employed. This is due to the fact that the proposed BDRC does not need accurate model information and features inherent robustness and high accuracy against various disturbances and internal/external uncertainties while the sliding mode control method needs very accurate turbine torque estimates. The proposed BDRC design does not need any differentials or suffer from the risks of explosion of complexity and high computational burden either.

VI. CONCLUSION

This paper designed a 160 kW two-stage tidal turbine system, analyzed its main characteristics, and developed an optimal tidal power generation control systems based on BDRC. The BDRC was synthesized in two control loops including an outer turbine dynamics control loop and an inner q-axis current dynamics control loop. An ESO and a nonlinear feedback controller were designed in each control loop. Both the stability and convergence of the two closed control loops and ESO were then analyzed. The effectiveness of the proposed BDRC in tracking the optimal tidal turbine speed and hence the optimal power generations have been verified based on simulations in Matlab Simulink. In addition, the proposed BDRC has been extended to general nonlinear strict-feedback systems with high uncertainties and external/internal disturbances and an entirely new control framework was then provided and analyzed, which indicates the proposed BDRC is a generic control approach and can be applicable to the control of a large range of nonlinear feedback systems. In the future, the proposed new control framework and its disturbance rejection ability will be validated through experimental work of large scale nonlinear feedback control systems, such as the tidal turbine control system.

VII ACKNOWLEDGEMENT

This work is supported by the UK Engineering and Physical Sciences Research Council (grant numbers: EP/S000747/1 and EP/R007470/1).

REFERENCES

[1] Segura, E., Morales, R., Somolinos, J. A., & López, A. (2017). Techno-economic challenges of tidal energy conversion systems: current status and trends. Renewable & Sustainable Energy Reviews, 77, 536-550.

[2] Winter A I. Differences in fundamental design drivers for wind and tidal turbines. OCEANS. 2011 IEEE-Spain. IEEE, 2011: 1-10.

[3] Payne, G. S., Stallard, T., & Martinez, R. (2017). Design and manufacture of a bed supported tidal turbine model for blade and shaft load measurement in turbulent flow and waves. Renewable Energy, 107, 312-326.

[4] Abdullah, M. A., Yatim, A. H. M., Tan, C. W., & Saidur, R. (2012). A review of maximum power point tracking algorithms for wind energy systems. Renewable & Sustainable Energy Reviews, 16(5), 3220-3227.

[5] Benelghali, S., Benbouzid, M. E. H., Charpentier, J. F., Ahmed-Ali, T., & Munteanu, I. (2010).

Experimental validation of a marine current turbine simulator: application to a permanent magnet synchronous generator-based system second-order sliding mode control. IEEE Transactions on Industrial Electronics, 58(1), 118-126.

[6] Elghali, S. E. B., Benbouzid, M. E. H., Ahmed-Ali, T., & Charpentier, J. F. (2010). High-order sliding mode control of a marine current turbine driven doubly-fed induction generator. IEEE Journal of Oceanic Engineering, 35(2), 402-411.

[7] Ben Elghali, S. E., Benbouzid, M. E. H., & Charpentier, J. F. (2010). Modelling and control of a marine current turbine-driven doubly fed induction generator. Renewable Power Generation IET, 4(1), 1-11.

[8] Chen, H., At-Ahmed, N., Machmoum, M., & Zam, E. H. (2015). Modeling and vector control of marine current energy conversion system based on doubly salient permanent magnet generator. IEEE Transactions on Sustainable Energy, 7(1), 409-418.

[9] Barakat, M. R., Tala-Ighil, B., Chaoui, H., Gualous, H., Slamani, Y., & Hissel, D. (2017). Energetic macroscopic representation of marine current turbine system with loss minimization control. IEEE Transactions on Sustainable Energy, PP (99), 1-1.

[10] Yin X, Lei M, Pan H. Direct optimal power extraction control for a tidal turbine system based on fuzzy power tuning. Ocean Engineering, 2018, 170: 426-433.

[11] Nambiar A, Anderlini E, Payne G S, et al. Reinforcement Learning Based Maximum Power Point Tracking Control of Tidal Turbines. Proceedings of the 12th European Wave and Tidal Energy Conference, Cork, Ireland. 2017, 27.

[12] Yin X, Zhao X. ADV Preview Based Nonlinear Predictive Control for Maximizing Power Generation of a Tidal Turbine With Hydrostatic Transmission. IEEE Transactions on Energy Conversion, 2019, 34(4): 1781-1791.

[13] Yin X, Zhao X. Sensorless Maximum Power Extraction Control of a Hydrostatic Tidal Turbine Based on Adaptive Extreme Learning Machine. IEEE Transactions on Sustainable Energy, 2019, 11(1): 426-435.

[14] Fraenkel, P. L. (2007). Marine current turbines: pioneering the development of marine kinetic energy

converters. Proceedings of the Institution of Mechanical Engineers Part A Journal of Power & Energy, 221(2), 159-169.

[15] Han J. From PID to active disturbance rejection control. IEEE transactions on Industrial Electronics, 2009, 56(3): 900-906.

[16] Huang Y, Xue W. Active disturbance rejection control: methodology and theoretical analysis. ISA transactions, 2014, 53(4): 963-976.

[17] Yao J, Deng W. Active disturbance rejection adaptive control of hydraulic servo systems. IEEE Transactions on Industrial Electronics, 2017, 64(10): 8023-8032.

[18] Sun B, Gao Z. A DSP-based active disturbance rejection control design for a 1-kW H-bridge DC-DC power converter. IEEE Transactions on Industrial Electronics, 2005, 52(5): 1271-1277.

[19] Sira-Ramírez H, Linares-Flores J, García-Rodríguez C, et al. On the control of the permanent magnet synchronous motor: an active disturbance rejection control approach. IEEE Transactions on Control Systems Technology, 2014, 22(5): 2056-2063.

[20] Chang X, Li Y, Zhang W, et al. Active disturbance rejection control for a flywheel energy storage system. IEEE Transactions on Industrial Electronics, 2014, 62(2): 991-1001.

[21] Cai Z, Lou J, Zhao J, et al. Quadrotor trajectory tracking and obstacle avoidance by chaotic grey wolf optimization-based active disturbance rejection control. Mechanical Systems and Signal Processing, 2019, 128: 636-654.

[22] Madonski R, Shao S, Zhang H, et al. General error-based active disturbance rejection control for swift industrial implementations. Control Engineering Practice, 2019, 84: 218-229.

[23] Sun L, Jin Y, You F. Active disturbance rejection temperature control of open-cathode proton exchange membrane fuel cell. Applied Energy, 2020, 261: 114381.

[24] Khan, N., Kalair, A., Abas, N., & Haider, A. (2017). Review of ocean tidal, wave and thermal energy technologies. Renewable & Sustainable Energy Reviews, 72, 590-604.

[25] Thomas, G. P. On the importance of wave – current interactions to tidal stream and marine current

generators. Fifth European Wave Energy Conference, University College Cork, Ireland, 17 –20 September 2003, 167 –174.

[26] Voulgaris G, Trowbridge JH. Evaluation of the acoustic Doppler velocimeter (ADV) for turbulence measurements. Journal of Atmospheric and Oceanic Technology, 1998, 15, 272-89.

[27] Whitby, B., & Ugalde-Loo, C. E. (2013). Performance of pitch and stall regulated tidal stream turbines. IEEE Transactions on Sustainable Energy, 5(1), 64-72.

[28] Slotine, J.-J. E. (Jean-Jacques E.), & Li, Weiping. (2004). Applied nonlinear control. Applied nonlinear control. China Machine Press.

[29] Li, J., Xia, Y., Qi, X., & Gao, Z. (2016). On the necessity, scheme and basis of the linear-nonlinear switching in active disturbance rejection control. IEEE Transactions on Industrial Electronics, PP (99), 1-1.

[30] Zhou, Q., Wu, C., Jing, X., & Wang, L. (2016). Adaptive fuzzy backstepping dynamic surface control for nonlinear input-delay systems. Neurocomputing, 199(C), 58-65.

[31] Ran M, Wang Q, Dong C, et al. Backstepping active disturbance rejection control: a delayed activation approach. IET Control Theory & Applications, 2017, 11(14): 2336-2342.